A Musculoskeletal Model of the Equine Forelimb for Determining Surface Stresses and Strains in the Humerus—Part I. Mathematical Modeling

Sarah Pollock
Biomedical Engineering Program,
University of California,
One Shields Avenue,
Davis, CA 95616

M. L. Hull[1]
Department of Mechanical Engineering,
and Biomedical Engineering Program,
University of California,
One Shields Avenue,
Davis, CA 95616
e-mail: mlhull@ucdavis.edu

Susan M. Stover
Department of Anatomy, Physiology and Cell Biology,
School of Veterinary Medicine,
and Biomedical Engineering Program,
University of California,
One Shields Avenue,
Davis, CA 95616

Larry D. Galuppo
Department of Anatomy, Physiology, and Cell Biology,
School of Veterinary Medicine,
University of California,
One Shields Avenue,
Davis, CA 95616

Knowledge of the forces that act upon the equine humerus while the horse is standing and the resulting strains experienced by the bone is useful for the prevention and treatment of fractures and for assessing the proximolateral aspect of the bone as a site for obtaining autogenous bone graft material. The first objective was to develop a mathematical model to predict the loads on the proximal half of the humerus created by the surrounding musculature and ground reaction forces while the horse is standing. The second objective was to calculate surface bone stresses and strains at three cross sections on the humerus corresponding to the donor site for bone grafts, a site predisposed to stress fracture, and the middle of the diaphysis. A three-dimensional mathematical model employing optimization techniques and asymmetrical beam analysis was used to calculate shoulder muscle forces and surface strains on the proximal and mid-diaphyseal aspects of the humerus. The active shoulder muscles, which included the supraspinatus, infraspinatus, subscapularis, and short head of the deltoid, produced small forces while the horse is standing; all of which were limited to 4.3% of their corresponding maximum voluntary contraction. As a result, the strains calculated at the proximal cross sections of the humerus were small, with maximum compressive strains of $-104\mu\varepsilon$ at the cranial aspect of the bone graft donor cross section. The middle of the diaphysis experienced larger strain magnitudes with compressive strains at the lateral and the caudal aspects and tensile strains at the medial and cranial aspects ($-377\mu\varepsilon$ and $258\mu\varepsilon$ maximum values, respectively) while the horse is standing. Small strains at the donor bone graft site do not rule out using this location to harvest bone graft tissue, although strains while rising to a standing position during recovery from anesthesia are unknown. At the site common to stress fractures, small strains imply that the stresses seen by this region while the horse is standing, although applied for long periods of time, are not a cause of fracture in this location. Knowing the specific regions of the middle of the diaphysis of the humerus that experience tensile and compressive strains is valuable in determining optimum placement of internal fixation devices for the treatment of complete fractures.
[DOI: 10.1115/1.2898726]

Introduction

Knowledge of the stresses and strains that the bones experience while the horse is standing, particularly the humerus, is important to improve the veterinary care and treatment of injuries to this bone. The high ground reaction loads developed during normal daily activities, such as walking and running [1,2], subject the skeletal system to complex internal loads that cause stresses and strains throughout the bones that may lead to fracture [3]. As a result of the high internal loads, stress fractures and complete fractures can develop in the forelimb bones of horses [4,5]. Specifically, the proximal end and diaphysis of the equine humerus are susceptible to cortical bone damage in the form of stress fractures and complete fractures due to the biomechanical overload experienced with training and racing [4,6]. Recovery from such injuries requires the horse to maintain a prolonged standing position during rehabilitation. Thus knowing the regions of the humerus that experience tensile and compressive strains while the horse is standing would assist in determining optimum placement of internal fixation devices for the treatment of complete fractures [7].

Knowledge of stresses and strains in the equine humerus during standing would also be useful because the proximolateral aspect of the bone, a site of relatively abundant and low fat cancellous bone tissue, has been proposed as a site for harvest of autogenous bone graft material [8]. In a study that evaluated the feasibility of obtaining donor bone from this location [8], one of the eight horses suffered a catastrophic fracture through the donor site during recovery from general anesthesia. It is possible that the cortical defect created in the humerus while obtaining cancellous graft material predisposed the bone to fracture through the development of a stress concentration at the harvest site.

Several methods have been used to assess stresses and strains developed in bones. Strain gauges have been used in vivo on equine bones with relatively easy surgical access [7,9–12] and in vitro on bones of the distal limb [13,14]. Finite element analysis [12,13] and mathematical models [9,12] have been also employed

[1]Corresponding author.

Contributed by the Bioengineering Division of ASME for publication in the JOURNAL OF BIOMECHANICAL ENGINEERING. Manuscript received May 10, 2006; final manuscript received July 10, 2007; published online May 29, 2008. Review conducted by Andrew A. Amis.

to study bones of the distal aspect of the limb in horses. To date, no methods known to the authors have been used to determine the strains on the equine humerus.

Because the equine humerus is not easily accessible for application of strain measuring devices, a simplified musculoskeletal model would greatly assist the identification of strains developed in the equine humerus as a result of ground reaction loads, surrounding musculature, and anatomical position. Consequently, the first objective of our study was to develop a mathematical model that would determine the loads on the proximal half of the humerus created by the surrounding musculature and ground reaction forces while the horse is standing. The second objective was to calculate surface bone stresses and strain magnitudes and directions at cross sections on the humerus corresponding to the donor site for bone graft, a site predisposed to stress fracture, and the middle of the diaphysis.

Methods

Mathematical Musculoskeletal Model. A right cadaveric forelimb of a 4-year-old Thoroughbred gelding (445 kg), euthanized for reasons unrelated to this study, was used to determine three-dimensional geometric data for the mathematical model. The specimen was transected just distal to the radius to isolate the proximal aspect of the limb, consisting of the scapula, humerus, radius, ulna, and associated soft tissues. The skin and subcutaneous tissue were removed. All muscles and ligaments either originating or inserting on the humerus were individually identified with the aid of anatomical references [15–17] and removed. A metallic marker was then embedded into each origin and insertion [18]. For large origins and insertions, a single metallic marker was placed at the centroid of each specific site as estimated from a previously dissected specimen and using anatomical references where muscles attach to bony prominences [16,17]. The biarticular biceps brachii muscle was marked at its origin on the scapula, insertion on the radius, and point of contact on the proximocranial aspect of the humerus. Other markers were placed on the bones to identify important landmarks, such as the humeral proximolateral donor site for bone graft, the humeral proximocaudal stress fracture site, contact points between the scapula and humerus and between the humerus and radius, and three cranial locations used to define the humeral coordinate system (see below). The axes of rotation in the sagittal and frontal planes of the shoulder and elbow joints were determined using the axis finder method [19] and also marked with metallic markers. The midpoint between the two markers corresponding to the lateral and medial surface locations of the axis of rotation of the shoulder joint in the sagittal plane was used to define the shoulder center of rotation for use in the mathematical model.

Once all relevant metallic markers were embedded, the bones were placed in an anatomical standing position (100 deg shoulder flexion angle, 135 deg elbow flexion angle) in the bed of a CT scanner (GE HighSpeed FX/i, Milwaukee, WI) (Fig. 1). A 2 mm helical CT scan (120 kVp, 100 mA) produced a total of 507 contiguous transverse images of the limb that were 2 mm thick with a 512×512 reconstruction matrix. From the continuously scanned CT images containing the transverse cross sections of the bones, the three-dimensional coordinates of each muscle's origin and insertion locations relative to one another were identified in a global CT coordinate system (Merge EFILM software, Milwaukee, WI).

To create a three-dimensional representation of force direction for each muscle during standing, an anatomically based coordinate system was constructed for the humerus using three planar contact points on the cranial side of the humerus (also marked with metallic markers prior to the CT scan). Two contact points located on the distal end of the humerus were the cranial aspect of the lateral (H_1) and medial (H_2) condyles. The third planar point on the intermediate ridge of the proximocranial aspect of the humerus (H_3) was located between the major and minor tubercles.

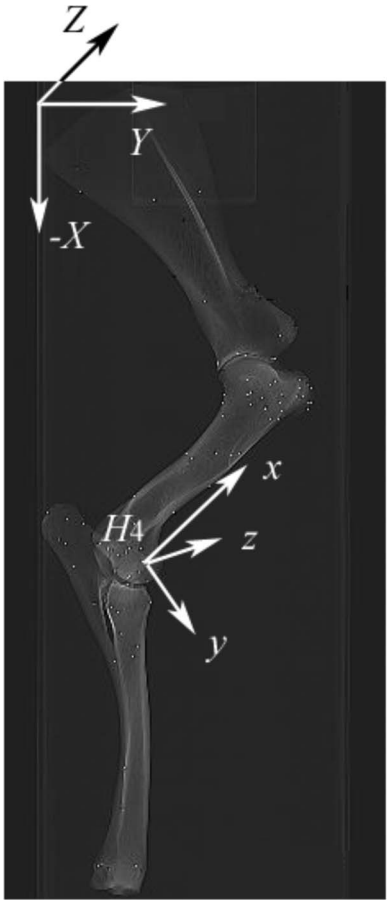

Fig. 1 Lateral CT scan of the scapula, humerus, radius, and ulna embedded with metallic markers to represent muscle origins and insertions, contact points, and other important locations. (X, Y, Z) represent the global CT coordinate system while (x, y, z) represent the local humeral coordinate system. The x axis was defined distal to proximal, the y axis was caudal to cranial, and the z axis was lateral to medial.

The origin of the local humeral coordinate system (H_4) was between the distal condyles and was calculated as the midpoint between H_1 and H_2. Unit vectors ($\hat{\mathbf{i}}, \hat{\mathbf{j}}, \hat{\mathbf{k}}$) of the local humeral coordinate system were defined as

$$\hat{\mathbf{i}} = \frac{\bar{\mathbf{r}}^{H_3/H_4}}{\left|\bar{\mathbf{r}}^{H_3/H_4}\right|}, \quad \hat{\mathbf{j}} = \frac{\hat{\mathbf{i}} \times \bar{\mathbf{r}}^{H_1/H_4}}{\left|\hat{\mathbf{i}} \times \bar{\mathbf{r}}^{H_1/H_4}\right|}, \quad \hat{\mathbf{k}} = \hat{\mathbf{i}} \times \hat{\mathbf{j}} \tag{1}$$

where the x axis was defined distal to proximal, the y axis was caudal to cranial, and the z axis was lateral to medial. In Eq. (1), the vector $\bar{\mathbf{r}}^{H_3/H_4}$ is the vector to point H_3 from point H_4. All 3D metallic marker coordinates were then transformed from the global CT coordinate system (X, Y, Z) to the origin of the humeral coordinate system (x, y, z) using a transformation matrix (Fig. 1).

Muscle locations relative to specific transverse cross sections of the humerus and muscle EMG data during the stance phase of walking were used as criteria to determine which shoulder muscles to include in the mathematical model. Transverse cross sections perpendicular to the longitudinal axis of the humerus were selected at the level of the bone graft donor, stress fracture, and mid-diaphyseal sites for analysis. Resultant loads occurring at the centroid of each cross section were calculated by analyzing all of the muscle and contact forces that were proximal to each of these cross sections (Fig. 2). Quadrupedal EMG data of equine [20] and canine [21] forelimb muscles during the stance phase of walking were also used to determine whether to include specific

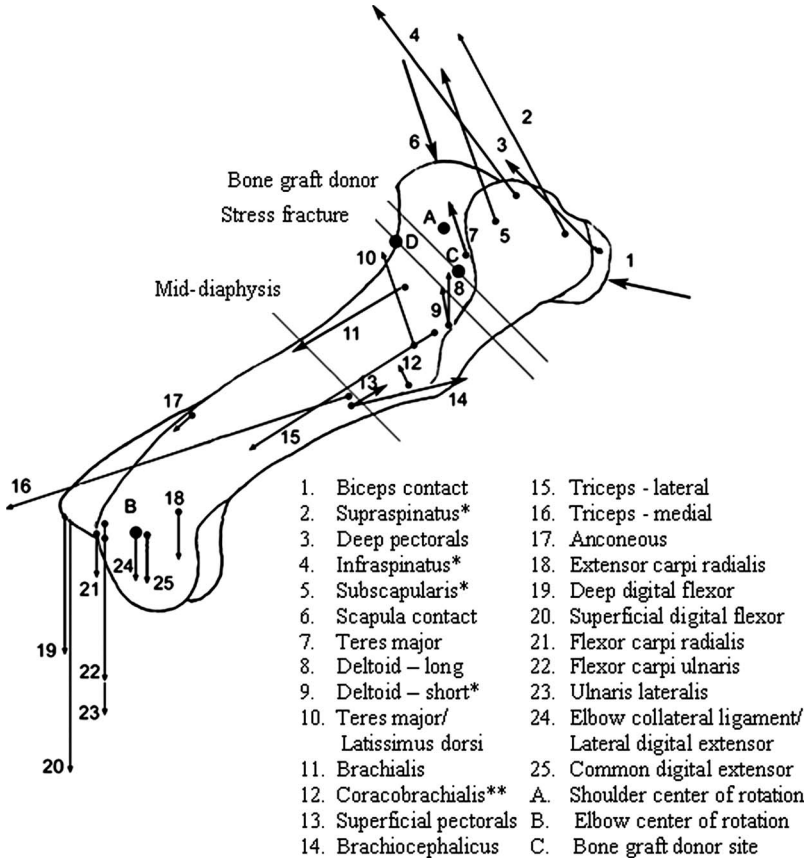

Fig. 2 Two-dimensional free body diagram of the equine humerus including forces due to muscles, bone-on-bone contact, and muscle wrapping contact, and transverse cross sections of the humerus corresponding to the bone graft donor site, stress fracture site, and middle of the diaphysis. Only muscles proximal to the middle of the diaphysis of the humerus and active during the middle of the stance phase of walking were used in the optimization procedure. * Active muscles during the middle of stance phase of walking as indicated by EMG data. ** Muscle for which no EMG data were available.

shoulder muscles in the mathematical model. EMG data from the stance phase of walking were used due to a lack of EMG data during standing. Muscles were included in the model if they were active according to EMG data and excluded if EMG data showed them to be quiescent. The resulting muscles used in the mathematical model included the supraspinatus, infraspinatus, subscapularis, teres minor, and short head of the deltoid.

Both the wrapping nature of the biceps brachii muscle and the bone-on-bone contact between the scapula and humerus produced contact forces acting on the proximal aspect of the humerus. The magnitude of the contact force exerted by the biceps brachii on the proximocranial aspect of the humerus was calculated using the results of a preliminary in vitro test loaded in a materials testing machine (MTS Systems Corp., Minneapolis, MN) (Fig. 3) where the goal was to load a simplified in vitro musculoskeletal preparation of the proximal forelimb consisting only of the scapula, humerus, radius, ulna, and biceps brachii muscle. The line of action of the contact force on the humerus from the scapula was assumed to run through the shoulder center of rotation (Fig. 4). Though the magnitude of the scapular contact force was unknown, it was calculated after the forces of the muscles that crossed the shoulder joint in the model were determined.

Intersegmental loads at the shoulder joint were calculated using lower limb segment masses and ground reaction loads acting at the center of the hoof based on a forelimb supporting 30% of the entire weight of the horse while standing [16]. The resulting intersegmental force and couple vectors, $\bar{\mathbf{F}}_e$ and $\bar{\mathbf{C}}_e$, respectively, acting at the center of the shoulder joint were calculated.

Constrained nonlinear static optimization techniques using sequential quadratic programming methods were used to solve the indeterminate problem of force sharing between shoulder muscles. Multiple randomized starting values were used to identify the global minimum. Constrained optimization was used to minimize the sum of the muscle stress cubed, which is thought to maximize muscular endurance [22], an important characteristic of equine limb muscles while a horse is standing for long periods of time. This method also better distributes force activity between numerous muscles while keeping individual muscle stresses low [23] instead of allocating large forces that directly correspond to muscles with larger physiologic cross-sectional areas. Optimized muscle force values were calculated using the following objective function and constraints:

Objective function,

$$\min \mathrm{U} = \sum_{i=1}^{m} \left(\frac{f_i}{\mathrm{PCSA}_i} \right)^3 \tag{2}$$

Inequality constraints,

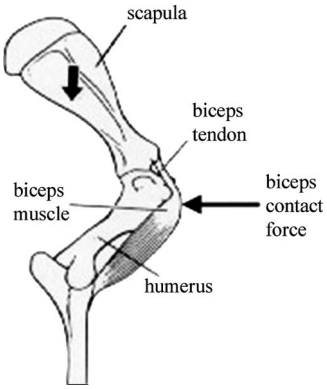

Fig. 3 Simplified musculoskeletal preparation for the biceps brachii only model used to calculate the biceps contact force. The large arrow on the scapula indicates the weight of the trunk of the horse (reprinted with permission [40] and biceps contact force added).

$$\frac{f_i}{\mathrm{PCSA}_i} \leqslant \sigma_{\max} \tag{3}$$

Equality constraint,

$$\sum_{i=1}^{m} (\bar{\mathbf{r}}_{im} \times \bar{\mathbf{f}}_{im}) = \bar{\mathbf{C}}_e \tag{4}$$

where m is the number of muscles, f_i, PCSA_i, and f_i/PCSA_i are the force, physiologic cross-sectional area, and the stress of the ith muscle, respectively, $\bar{\mathbf{r}}_{im}$ is the vector originating from the shoulder center of rotation to the respective origin or insertion of the ith muscle, and $\bar{\mathbf{f}}_{im}$ is the force vector of the ith muscle. Because PCSA values for equine shoulder muscles have not been reported, PCSA values were estimated during gross dissection where muscle volumes and the length and orientation of muscle fibers were determined. The maximum allowable stress limit for each muscle, $\sigma_{\max}$, was set to the maximum physiologically achievable muscle stress, 350 kPa, as recommended by Zajac [24]. Predicted muscle forces were compared to maximum voluntary contraction (MVC) values calculated using PCSA and a specific tension of 15 $\mathrm{N/cm^2}$ [25,26]. Finally, the scapular contact force was computed from

$$\bar{\mathbf{F}}_e = \sum_{i=1}^{m} \bar{\mathbf{f}}_{im} + \sum_{j=1}^{c} \bar{\mathbf{f}}_{jc} \tag{5}$$

where c is the number of contact points and $\bar{\mathbf{f}}_{jc}$ is the force vector of the jth contact. Note that no ligament forces were included in Eq. (5) because no ligaments cross the equine shoulder joint.

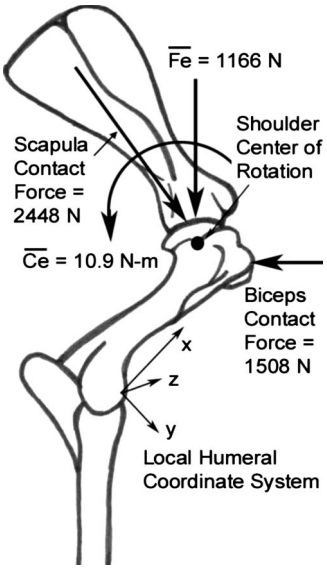

Fig. 4 Intersegmental force ($\bar{\mathbf{F}}_e$) and couple ($\bar{\mathbf{C}}_e$) vectors, and contact forces due to the biceps brachii muscle and the scapula exerted on the proximal humerus

Table 1 Forces in equine shoulder muscles while standing predicted using optimization techniques that minimized the sum of muscle stress cubed. For each muscle, force values are compared to MVC.

Muscle	Force (N)	Calculated MVC (N)	Percentage of MVC
Subscapularis	144	3525	4.1
Supraspinatus (lateral head)	57	1326	4.3
Supraspinatus (medial head)	40	1326	3.0
Infraspinatus	73	3807	1.9
Teres minor	0	440	0.0
Deltoid (short head)	2	274	0.7

Stress and Strain Calculations. The geometry and material properties of the three transverse cross sections of interest on the humerus were used to calculate surface bone stresses. The centroid, moments of inertia, and product of inertia were calculated for the cortical bone in each transverse cross section [27], and the resultant force and moment vectors due to the shoulder muscle forces and contact forces while standing were calculated at the centroid of each cross section. The components of the resultant force vector were the axial compressive force (F_x) and the two shear forces (F_y and F_z). The components of the resultant moment vector were the torsional moment (M_x) and the bending moments (M_y and M_z). The calculated force and moment components specific to a transverse cross section were then used to determine the stresses occurring on the cortical bone surface in various locations around the cross-sectional perimeter.

Assuming a prismatic beam and using asymmetrical beam analysis for the cortical bone shell of the humerus, surface stresses were calculated at the bone graft donor and stress fracture sites and at the lateral, medial, caudal, and cranial aspects of each transverse cross section due to the axial compression and bending in the frontal (M_y) and sagittal (M_z) planes [12,28,29]. Each stress value was then used to calculate the corresponding strain using Hooke's law. In these calculations, E is the elastic modulus = 18 GPa, representing the inherent stiffness of the cortical bone, and ν is Poisson's ratio = 0.3 [12].

Results

Mathematical Model. The forces predicted using optimization techniques for the equine shoulder muscles were 4.3% or less than their corresponding MVC, with a maximum muscle force of 144 N calculated for the subscapularis muscle (Table 1). The magnitudes of the intersegmental force and couple vectors calculated through the center of rotation of the shoulder included a 1166 N vertical force and a 10.9 N m couple in the direction of shoulder flexion in the sagittal plane (Fig. 4). The force exerted by the biceps brachii contact at the proximocranial aspect of the humerus was 1508 N in magnitude. The force due to the contact from the proximally located scapula was 2448 N in magnitude (Fig. 4).

Stress and Strain Calculations. The geometric properties of the transverse cross section at the middle of the diaphysis of the

Table 2 Geometric properties of the three cross sections of the humerus, including moments of inertia, product of inertia, and area of cortical bone (the *x* axis is the long axis of the bone)

Cross section	*Iyy* (cm^4)	*Izz* (cm^4)	*Iyz* (cm^4)	Cortical bone area (cm^2)
Bone graft donor	76.0	111.7	−24.5	8.97
Stress fracture	44.7	59.0	−29.4	7.69
Mid-diaphysis	35.0	41.3	−13.4	15.03

humerus included smaller inertia quantities notwithstanding a cortical bone area nearly twice that of the bone graft donor and the stress fracture cross sections (Table 2). The addition of the short head of the deltoid muscle to the force calculations at the centroid of the mid-diaphyseal transverse cross section did not considerably alter the calculated forces (Table 3). The resultant moment at the centroid of each transverse cross section increased in magnitude as the cross section was shifted from a proximal (bone graft donor) to a distal (mid-diaphyseal) location on the humerus (Table 3). At the same time, the directions of the moment components differed at each of the three cross sections (Table 3, Fig. 5).

The normal stresses calculated in the direction of the longitudinal axis at the middle of the diaphysis of the humerus were greater in magnitude than those calculated at the more proximally located transverse cross sections containing the stress fracture site and the bone graft harvest site (Table 4). Either negligible or compressive stresses were found around the perimeter of the bone graft donor

Table 3 Force and moment components calculated at the centroids of the bone graft donor, stress fracture, and mid-diaphyseal cross sections. Values are forces and moments in terms of the local humeral coordinate system.

Bone graft donor cross section		
Forces (N)	F_x	831
	F_y	−803
	F_z	−177
	Resultant force	1169
Moments (N m)	M_x	−0.5
	M_y	3.5
	M_z	−18.1
	Resultant moment	18.4
Stress fracture cross section		
Forces (N)	F_x	831
	F_y	−803
	F_z	−177
	Resultant force	1169
Moments (N m)	M_x	−12.1
	M_y	−10.8
	M_z	−8.2
	Resultant moment	18.2
Mid-diaphysis cross section		
Forces (N)	F_x	829
	F_y	−801
	F_z	−177
	Resultant force	1166
Moments (N m)	M_x	8.7
	M_y	−6.8
	M_z	71.3
	Resultant moment	72.1

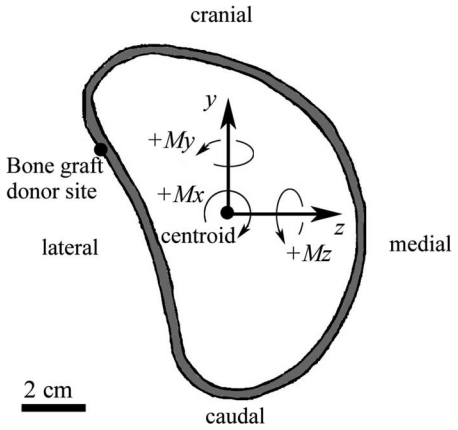

Fig. 5 Transverse cross section of a right humerus at the level of the bone graft donor site viewed from the bottom in the direction of the positive *x* axis. The positive torsional moment (M_x) and the bending moments (M_y and M_z) are labeled at the centroid of the cross section, and the shaded region represents cortical bone.

transverse cross section. The lateral, medial, caudal, and cranial aspects of the stress fracture cross section were in compression. At the middle of the diaphysis, compressive stresses were found at the lateral and caudal aspects and tensile stresses at the medial and cranial aspects. Normal stresses at the specific location of the bone graft donor site on the proximolateral aspect of the bone graft donor transverse cross section and at the specific stress fracture site were negligible (−1.0 MPa and −0.6 MPa compressive stresses, respectively). Finally, the trends in the strain magnitudes calculated at the lateral, medial, caudal, and cranial aspects of the bone graft donor, stress fracture, and mid-diaphyseal transverse cross sections mimicked the trends in the stress values calculated at these locations (Table 4).

Discussion

Knowledge of the forces that act upon the equine humerus while the horse is standing and the resulting strains experienced

Table 4 Humeral stresses and strains at the bone graft donor, stress fracture, and mid-diaphyseal cross sections. Locations include the lateral, medial, caudal, and cranial aspects of each cross section, in addition to the specific bone graft donor site and stress fracture site. Compressive values are negative and tensile values are positive.

Cross section	Location	Stress σ_x (MPa)	Strain ε_x ($\mu\varepsilon$)
Bone graft donor	Bone graft donor site	−1.0	−56
	Lateral	−0.6	−35
	Medial	−1.4	−77
	Caudal	0.1	6
	Cranial	−1.9	−104
Stress fracture	Stress fracture site	−0.6	−35
	Lateral	−1.5	−85
	Medial	−0.3	−16
	Caudal	−1.0	−54
	Cranial	−1.2	−65
Mid-diaphysis	Lateral	−3.0	−169
	Medial	1.9	107
	Caudal	−6.8	−377
	Cranial	4.6	258

by the bone are useful for preventing fracture, appropriately applying implants to stabilize complete humeral fracture, and to evaluate the proximolateral aspect of the bone as a site for obtaining autogenous bone graft material. Thus one objective of our study was to develop a mathematical model that would determine the loads on the proximal half of the humerus while the horse is standing. A second objective was to calculate surface bone stresses and strain magnitudes and directions at cross sections on the humerus corresponding to the donor site for bone grafts, a site predisposed to stress fracture, and the middle of the diaphysis. One key finding was that the shoulder muscles activated while the horse is standing include the subscapularis, supraspinatus, infraspinatus, and a minor activation of the short head of the deltoid. These muscles produce very small forces however, which are limited to 4.3% or less of their corresponding MVC. A second key finding was that the strains occurring at the more proximal cross sections of the humerus corresponding to the bone graft donor and stress fracture transverse cross sections were either small or negligible. The middle of the diaphysis experienced larger strain magnitudes with compressive strains at the lateral and the caudal aspects and tensile strains at the medial and cranial aspects.

The computed stresses and strains at the different locations on the equine humerus are potentially useful. Negligible strains at the donor bone graft site do not rule out this location as a site for introducing a hole to harvest bone graft tissue provided that potentially large strains that might occur during recovery from anesthesia are avoided. At the site common to stress fractures, negligible stresses and strains imply that the stresses seen by this region while the horse is standing, although applied for long periods of time, are not a cause of fracture in this location. Because the efficacy of an internal fixation device is dependent on location of tensile strains experienced where the plate is attached to the bone [7], it is valuable to know that tensile strains occur at the medial and cranial aspects and compressive strains occur at the lateral and caudal aspects of the middle of the diaphysis of the humerus while the horse is standing. Ultimately, validation of the stresses and strains calculated using the mathematical model is necessary before direct recommendations are made using these data.

The low muscle forces predicted using the mathematical model reinforces the idea that the horse supports its body weight with minimal muscular effort while standing. This also supports the idea that the objective function used in the model (minimizing the sum of muscle stress cubed) predicted individual muscle forces that maximized muscular endurance [22]. All muscle forces predicted using the model were extremely small when compared to maximum voluntary muscle contraction as determined by specific tension and each muscle's physiologic cross-sectional area.

Because strains have not been previously studied in the equine humerus, a direct comparison of the values calculated using the mathematical model is not possible. Strains have been tested on other equine bones using strain gauges, both in vivo [7,9–12] and in vitro [13,14]. Humeral surface strains calculated at the middle of the diaphysis in this study are similar in magnitude and direction to strains found on the diaphysis of the equine tibia when tested in vivo with strain gauges while the horse was standing [7].

Considering that the stresses and strains were computed using a new biomechanical model, it is useful to critically assess various aspects of the model development to gain confidence in model results. Including the 1508 N contact force created by the biceps brachii muscle at the proximocranial aspect of the humerus was essential for calculating loads at the various transverse cross sections of interest, and resulting stresses and strains. The biceps brachii crosses the shoulder and elbow joints of the forelimb and contains an internal tendon that runs the entire length of the muscle. This strong muscle-tendon complex can extend the shoulder joint, flex the elbow joint, and/or prevent excessive flexion of the shoulder joint during elbow extension depending on limb position during gait and stance [30]. The biceps brachii neither originates nor inserts on the humerus. Thus tension of the muscle applies pressure via its contact on the proximocranial aspect of the obliquely oriented humerus, thereby allowing the weight of the cranial end of the trunk to be transferred to the vertically oriented radius in the standing horse [30]. The biceps brachii, with its internal tendon, is also an integral part of the passive-stay apparatus, which allows the horse to support its large body weight on its feet for long periods of time with minimal muscular effort [16].

The triceps muscle was not included in the model because it extends the elbow to position the forelimb in the stay apparatus for standing but then relaxes during standing. As a result, it is not actively contracting while the horse is standing. This is also supported by the fact that EMG data for the triceps muscle are negligible during the middle of the stance phase of walking [20,21]. In addition, the long head of the triceps brachii, which comprises the bulk of the muscle, attaches to the scapula and the ulna and does not attach to the humerus.

Due to lack of forelimb muscle EMG data while the horse is standing, EMG data from the middle of stance phase of walking were used [20,21]. It was assumed that forelimb conformation during standing was comparable to forelimb conformation during the middle of stance phase of walking. In addition, the muscles involved in standing were assumed to be a subset of the muscles that are active during the stance phase of walking because walking is a more complicated action.

The 15 N/cm^2 specific tension value used to calculate muscle MVC may not have accurately depicted the maximum force that each muscle can actually generate. Specific tension may vary among muscle fiber types and between species [31]; slow, oxidative muscle fibers generally have a lower specific tension than that of fast, glycolytic fibers. Values reported in literature have a range of 15.7–29.4 N/cm^2 for mammalian muscle [32], 8–11 N/cm^2 for human flexor muscles [33], and 8–12 N/cm^2 for equine soleus muscle [34]. Because the muscles used in this mathematical model function to extend and stabilize the shoulder joint, they were assumed to be primarily composed of slow, oxidative fibers. Therefore, a submaximal value was chosen for specific tension in this study and, as a result, the muscle forces calculated in the model may be a larger percentage of the MVC than if a larger specific tension value would have been used.

To calculate normal stresses for the cortical bone shell of the humerus from predicted muscle forces, asymmetrical beam analysis was chosen. Other studies that have used beam theory for three-dimensional mathematical stress analysis are limited to studies on the midshaft of long bones [28,35–37]. A comparative study of beam analysis versus finite element analysis argued that beam analysis is appropriate for the calculation of the stresses in the shaft of the human femur, but a continuum model should be used for the upper and lower regions of the femur, as well as sites of muscle attachment [28]. Although the equine humerus is relatively short, the insertion sites for muscles used in this model are more proximal than locations on the humerus where stresses were analyzed thus lending promise to the use of the beam analysis for the purposes of our study. Asymmetrical beam analysis has not currently been employed to identify stresses in this region of the horse.

In computing strains, the material properties of the bone were required. First, it was assumed that the stresses occurring on the surface of the humerus were unaffected by the material properties of the cancellous bone because the elastic modulus of the cancellous bone ($E=1$ GPa) [38] was much smaller than that of the cortical bone ($E=18$ GPa) [12]. Second, the material properties of the cortical bone shell of the humerus were assumed to be both isotropic and homogeneous [39]. Although bone is an anisotropic material with strength and material properties varying in the longitudinal and transverse directions, these values have not been classified for the equine humerus and, therefore, the effects of mathematically analyzing the equine humerus as anisotropic in a mathematical model have not been tested. Third, the 18 GPa value

used for the elastic modulus [12] may have underestimated some of the calculated strain magnitudes particularly at the middle of the diaphysis because the elastic modulus may be greater at this location than at the proximal locations.

The effects of torsion and shear forces were assumed to be negligible. This assumption was reasonable based on stress calculations performed on a prismatic cylinder with a cross-sectional area similar to that of the equine humerus. At the location of the bone graft donor site, the stress due to the axial compression was −1.1 MPa and the stress due to bending was 0.6 MPa, whereas the stress due to torsion was −0.01 MPa and the stress due to the shear forces was zero.

In summary, the results of this study indicate that the equine shoulder muscles are not highly activated while the horse is standing. Such low muscle forces do not significantly strain the proximal aspects of the humerus and produce strains at the middle of the diaphysis that are comparable to strains found in another in vivo study [7]. The results of this study can possibly be used to help prevent and treat fractures at specific locations on the equine humerus. Although the assumptions used to develop the model are reasonable, it is important to experimentally test the validity of the model to make dependable recommendations from the calculations made in this study. Therefore, experimental validation of this musculoskeletal model is investigated in vitro as described in Part II of this paper [41].

Acknowledgment

Funding was provided by a grant from the Center for Equine Health at the University of California, Davis. The authors would also like to thank Tanya Garcia-Nolan and Ken Taylor for contributions to this work.

References

[1] Brown, N. A., Pandy, M. G., Kawcak, C. E., and McIlwraith, C. W., 2003, "Force- and Moment-Generating Capacities of Muscles in the Distal Forelimb of the Horse," J. Anat., **203**(1), pp. 101–113.

[2] Hodson, E., Clayton, H. M., and Lanovaz, J. L., 2000, "The Forelimb in Walking Horses: 1. Kinematics and Ground Reaction Forces," Equine Vet. J., **32**(4), pp. 287–294.

[3] Markel, M. D., 1996, "Fracture Biomechanics," *Equine Fracture Repair*, A. J. Nixon, ed., W. B. Saunders Co., Philadelphia, PA, pp. 10–18.

[4] Nixon, A. J., and Watkins, J. P., 1996, "Fractures of the Humerus," *Equine Fracture Repair*, A. J. Nixon, ed., W. B. Saunders Co., Philadelphia, PA, pp. 242–253.

[5] Nunamaker, D. M., Butterweck, D. M., and Provost, M. T., 1990, "Fatigue Fractures in Thoroughbred Racehorses: Relationships With Age, Peak Bone Strain, and Training," J. Orthop. Res., **8**(4), pp. 604–611.

[6] Stover, S. M., Johnson, B. J., Daft, B. M., Read, D. H., Anderson, M., Barr, B. C., Kinde, H., Moore, J., Stoltz, J., Ardans, A. A., and Pool, R. R., 1992, "An Association Between Complete and Incomplete Stress Fractures of the Humerus in Racehorses," Equine Vet. J., **24**(4), pp. 260–263.

[7] Turner, A. S., Mills, E. J., and Gabel, A. A., 1975, "In Vivo Measurement of Bone Strain in the Horse," Am. J. Vet. Res., **36**(11), pp. 1573–1579.

[8] Harriss, F. K., Galuppo, L. D., Decock, H. E., McDuffee, L. A., and Macdonald, M. H., 2004, "Evaluation of a Technique for Collection of Cancellous Bone Graft From the Proximal Humerus in Horses," Vet. Surg., **33**(3), pp. 293–300.

[9] Rybicki, E. F., and Mills, E. J., 1977, "In Vivo and Analytical Studies of Forces and Moments in Equine Long Bones," J. Biomech., **10**(11/12), pp. 701–705.

[10] Hartman, W., Schamhardt, H. C., Lammertink, J. L., and Badoux, D. M., 1984, "Bone Strain in the Equine Tibia: An In Vivo Strain Gauge Analysis," Am. J. Vet. Res., **45**(5), pp. 880–884.

[11] Biewener, A. A., Thomason, J., Goodship, A., and Lanyon, L. E., 1983, "Bone Stress in the Horse Forelimb During Locomotion at Different Gaits: A Comparison of Two Experimental Methods," J. Biomech., **16**(8), pp. 565–576.

[12] Gross, T. S., McLeod, K. J., and Rubin, C. T., 1992, "Characterizing Bone Strain Distributions In Vivo Using Three Triple Rosette Strain Gages," J. Biomech., **25**(9), pp. 1081–1087.

[13] Les, C. M., Keyak, J. H., Stover, S. M., and Taylor, K. T., 1997, "Development and Validation of a Series of Three-Dimensional Finite Element Models of the Equine Metacarpus," J. Biomech., **30**(7), pp. 737–742.

[14] Fleck, C., and Eifler, D., 2003, "Deformation Behaviour and Damage Accumulation of Cortical Bone Specimens From the Equine Tibia Under Cyclic Loading," J. Biomech., **36**(2), pp. 179–189.

[15] Barone, R., 1976, *Anatomie Comparee Des Mammiferes Domestiques, Tome I Osteologie*, 2nd ed., Vigot, Paris, France, pp. 272–290.

[16] Dyce, K. M., Sack, W. O., and Wensing, C. J. G., 2002, *Textbook of Veterinary Anatomy*, 3rd ed., Elsevier Science, Philadelphia, PA, pp. 568–605.

[17] Pasquini, C., 1991, *Atlas of Equine Anatomy, Regional Approach*, 3rd ed., SUDZ, Pilot Point, TX, pp. 166–210.

[18] Brand, R. A., Crowninshield, R. D., Wittstock, C. E., Pedersen, D. R., Clark, C. R., and van Krieken, F. M., 1982, "A Model of Lower Extremity Muscular Anatomy," ASME J. Biomech. Eng., **104**(4), pp. 304–310.

[19] Hollister, A. M., Jatana, S., Singh, A. K., Sullivan, W. W., and Lupichuk, A. G., 1993, "The Axes of Rotation of the Knee," Clin. Orthop. Relat. Res., **290**, pp. 259–268.

[20] Korsgaard, E., 1982, "Muskelfunktionen I Hestens Forben, En Elektromyografisk Og Kinesiologisk Undersogelse," Ph.D. Thesis, De. Kgl. Veterinaer—og Landbohojskole, Institut for Kirurgi, Kobenhavn, Denmark.

[21] Tokuriki, M., 1973, "Electromyographic and Joint-Mechanical Studies in Quadrupedal Locomotion. I. Walk," Nippon Juigaku Zasshi, **35**(5), pp. 433–436.

[22] Crowninshield, R. D., and Brand, R. A., 1981, "A Physiologically Based Criterion of Muscle Force Prediction in Locomotion," J. Biomech., **14**(11), pp. 793–801.

[23] Berme, N., Heydinger, G., and Cappozzo, A., 1987, "Calculation of Loads Transmitted at the Anatomical Joints," *Biomechanics of Engineering: Modeling, Simulation, Control*, A. Morecki, ed., Springer, Wien, NY, pp. 89–131.

[24] Zajac, F. E., 1989, "Muscle and Tendon: Properties, Models, Scaling, and Application to Biomechanics and Motor Control," Crit. Rev. Biomed. Eng., **17**(4), pp. 359–411.

[25] Swanstrom, M. D., Zarucco, L., Stover, S. M., Hubbard, M., Hawkins, D. A., Driessen, B., and Steffey, E. P., 2005, "Passive and Active Mechanical Properties of the Superficial and Deep Digital Flexor Muscles in the Forelimbs of Anesthetized Thoroughbred Horses," J. Biomech., **38**(3), pp. 579–586.

[26] Lieber, R. L., 2002, *Skeletal Muscle Structure, Function, and Plasticity*, 2nd ed., Lippincott Williams & Wilkins, Baltimore, MD, pp. 45–112.

[27] Koch, J. C., 1917, "The Laws of Bone Architecture," Am. J. Anat., **21**(2), pp. 177–298.

[28] Rybicki, E. F., Simonen, F. A., and Weis, E. B., Jr., 1972, "On the Mathematical Analysis of Stress in the Human Femur," J. Biomech., **5**(2), pp. 203–215.

[29] Ugural, A. C., and Fenster, S. K., 1987, *Advanced Strength and Applied Elasticity*, 2nd SI ed., Elsevier Science, New York, NY, pp. 135–143.

[30] Nevens, A. L., Stover, S. M., and Hawkins, D. A., 2005, "Evaluation of the Passive Function of the Biceps Brachii Muscle-Tendon Unit in Limitation of Shoulder and Elbow Joint Ranges of Motion in Horses," Am. J. Vet. Res., **66**(3), pp. 391–400.

[31] Lieber, R. L., 1999, "Skeletal Muscle Is a Biological Example of a Linear Electro-Active Actuator," *Proceedings of the SPIE's 6th Annual International Symposium on Smart Structures and Materials*, Mar. 1–5, San Diego, CA, Paper No. 3669-03, pp. 19–25.

[32] Powell, P. L., Roy, R. R., Kanim, P., Bello, M. A., and Edgerton, V. R., 1984, "Predictability of Skeletal Muscle Tension From Architectural Determinations in Guinea Pig Hindlimbs," J. Appl. Physiol., **57**(6), pp. 1715–1721.

[33] Fukunaga, T., Roy, R. R., Shellock, F. G., Hodgson, J. A., and Edgerton, V. R., 1996, "Specific Tension of Human Plantar Flexors and Dorsiflexors," J. Appl. Physiol., **80**(1), pp. 158–165.

[34] Rome, L. C., Sosnicki, A. A., and Goble, D. O., 1990, "Maximum Velocity of Shortening of Three Fibre Types From Horse Soleus Muscle: Implications for Scaling With Body Size," J. Physiol. (London), **431**, pp. 173–185.

[35] Toridis, T. G., 1969, "Stress Analysis of the Femur," J. Biomech., **2**(2), pp. 163–174.

[36] Piotrowski, G., and Wilcox, G. A., Jr., 1971, "The Stress Program: A Computer Program for the Analysis of Stresses in Long Bones," J. Biomech., **4**(6), pp. 497–506.

[37] Lieberman, D. E., Polk, J. D., and Demes, B., 2004, "Predicting Long Bone Loading From Cross-Sectional Geometry," Am. J. Phys. Anthropol., **123**(2), pp. 156–171.

[38] Nigg, B. M., and Grimston, S. K., 1994, "Bone," *Biomechanics of the Musculo-Skeletal System*, B. M. Nigg and W. Herzog, eds., Wiley, Chichester, NY, pp. 61–62.

[39] Cordey, J., and Gautier, E., 1999, "Strain Gauges Used in the Mechanical Testing of Bones. Part I: Theoretical and Technical Aspects," Injury, **30**(1), pp. A7–A13.

[40] MacFadden, B., 1993, "How Can Horses Stand for So Long?," *Florida Fossil Horse Newsletter*, Florida Museum of Natural History, Gainesville, FL, Vol. 2, Issue 4, http://www.flmnh.ufl.edu/ponyexpress/pony2_4/Pe24.htm

[41] Pollock, S., Stover, S. M., Hull, M. L., and Galuppo, L. D., 2008, "A Musculoskeletal Model of the Equine Forelimb for Determining Stresses and Strains in the Humerus—Part II. Experimental Testing and Model Validation," ASME J. Biomech. Eng., **130**, p. 041007.